ADVANCED FUNCTIONAL MATERIALS
www.afm-journal.de



# Profile Control in Block Copolymer Nanostructures using Bilayer Thin Films for Enhanced Pattern Transfer Processes

*Chunlin He and Mark P. Stoykovich**

**Although control over the domain orientation and long-range order of block copolymer nanostructures self-assembled in thin films has been achieved using various directed self-assembly techniques, more challenging but equally important for many lithographic applications is the ability to precisely control the shape of the interface between domains. Here, a novel layer-by-layer approach is reported for controlling the interface profile of block copolymer nanostructures and the application of an undercut sidewall profile for an enhanced metal lift-off process for pattern transfer is demonstrated. Bilayer films of lamellar-forming poly(styrene-*block*-methyl methacrylate) are assembled and thermally cross-linked on wafer substrates in a layer-by-layer process. The top layer, while being directed to self-assemble on the lamellae of the underlying layer, has a tunable composition and polystyrene domain width independent of that of the bottom layer. Undercut or negative sidewall profiles in the PS nanostructures are proven to provide better templates for the lift-off of Au nanowires by achieving complete and defect-free pattern transfer more than three times faster than comparable systems with vertical sidewall profiles. More broadly, the layer-by-layer approach presented here provides a pathway to achieving sophisticated interface profiles and user-defined 3D block copolymer nanostructures in thin films.**

## 1. Introduction

Block copolymer self-assembly in thin films spontaneously generates nanostructured patterns, however, for many lithographic applications the pattern must be transferred to a functional electronic,[1] optical,[2] or magnetic material.[3] Thus the block copolymer nanostructures often mimic a patterned photoresist film, serving as a template for the deposition of the functional materials or as a mask for substrate etching. Pattern transfer processes using block copolymer nanostructures have been challenging, due in part to the thin films that are used (e.g., usually <100 nm as required to maintain low feature aspect ratios[4]), the less than ideal polymeric constituents (e.g., common block copolymer systems provide poor etch resistance[4,5]), and a lack of structural and interfacial control. Lift-off processes for the additive vapor-phase deposition of materials using conventional lithographic techniques, for example, benefit from photoresist patterns with an undercut or negative sidewall profile as illustrated in **Figure 1**.[6] Selective removal of the deposited material from the photoresist protected regions is facilitated during lift-off by the undercut profile preventing continuous coverage over the substrate and photoresist features. Photoresist structures with an undercut profile therefore serve two purposes: first they allow solvent to directly access and dissolve the photoresist and second they let the unconnected material freely float away and be removed. Lift-off using photoresist structures with vertical or positive sidewall profiles (see Figure 1) may be slow, may be troubled by retention or inhomogeneous pattern transfer across the substrate,[7] and can lead to rough edges or "ears" on the patterned material.[8] In conventional photoresists, undercut profiles are achieved through careful design of the molecular composition of the photoresist (e.g., negative versus positive tone)[9] or the development of special processing conditions (e.g., via the exposure dose or presoaking the photoresist film in solvent to create a gradient in relative solubility).[6] Alternatively, bilayer photoresist films[10] are often used to achieve T-top shaped structures (see Figure 1), with the top layer being less soluble than the underlying layer at the given exposure and development conditions.

The control of sidewall profiles in block copolymer nanostructures is inherently more difficult. Block copolymer structures oriented perpendicular to the substrate have interfacial shapes dictated by the thermodynamics of the system and preferentially adopt vertical sidewall profiles.[11] In many cases this is an attractive feature of self-assembly, such that block copolymer structures have been shown to provide critical dimension control,[12] to self-heal defects,[13] and to reduce line edge roughness.[14] Here we have developed an approach, analogous to that in bilayer photoresist films, to achieve tunable interface shapes and sidewall profiles in block copolymer nanostructures in thin films. It is demonstrated that such interfacial control provides the unique opportunity to design block copolymer nanostructures specially tuned for pattern transfer, including lift-off processes.

C. He, Prof. M. P. Stoykovich
Department of Chemical and Biological Engineering
University of Colorado at Boulder
Boulder, CO 80309, USA
E-mail: mark.stoykovich@colorado.edu

DOI: 10.1002/adfm.201401810

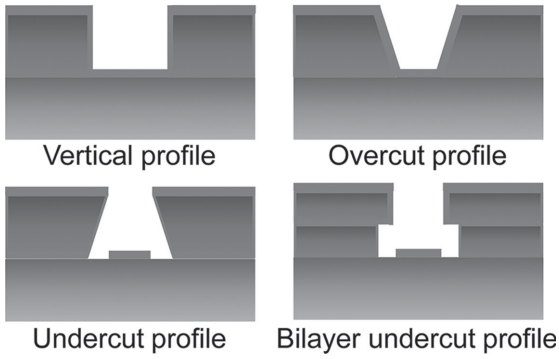


**Figure 1.** Common sidewall profiles of photoresist structures after lithographic patterning.

## 2. Results and Discussion

The step-by-step schematic in **Figure 2** illustrates our approach to control the sidewall profiles of block copolymer nanostructures through the use of bilayer self-assembled thin films. Briefly, block copolymer thin films were deposited on a neutral brush treated surface and solvent annealed under a mixed solvent vapor leading to the self-assembly of lamellae oriented perpendicular to the substrate.[15] A cross-linking reaction was subsequently performed within the self-assembled domains by heating the sample to 190 °C for 1 h. The resulting cross-linked nanostructures were thus fixed and became relatively insoluble. A second layer of block copolymer could then be deposited and processed under identical conditions (i.e., self-assembly via solvent annealing followed by cross-linking upon thermal treatment). In this manner, the underlying first layer served as a chemically patterned substrate that directed the self-assembly of the block copolymer structures in the second layer.[16] Individual block copolymer layers were ≈25 nm thick, thereby generating a nanostructured film with a total thickness of 50 nm. The system used here consisted of polystyrene (PS) and poly(methyl methacrylate) (PMMA) components, which is advantageous because it is a well-characterized, model block copolymer system[17] and the PMMA domain can be selectively removed through standard processes.[18] This approach can be generalized to most block copolymers systems, but other such materials may exhibit subtle differences in the structures self-assembled in thin films from those presented here due to more disparate domain surface tensions than in the PS/PMMA system (e.g., it may be more difficult to achieve perpendicular interfaces and nanostructures even on a neutral surface).

A multilayer approach to controlling the interface profiles of block copolymer nanostructures allows the composition, and thus dimension, of each self-assembled layer to be adjusted independently. In this study, negative or undercut sidewall profiles in the PS domain were targeted in order to enhance the success of such self-assembled nanostructures to serve as a mask for lift-off processes for pattern transfer. This type of profile in a block copolymer nanostructure requires that each layer have the same periodicity but differing domain widths. Such an undercut profile was fabricated from a bilayer thin film, with the bottom layer having a PS volume fraction ($\phi_{PS}$) of 50.0 vol% and the top layer having $\varphi_{PS}$ = 60.0 vol%, as indicated by the notation "Bilayer 50–60PS" used in this manuscript. Each layer consisted of a block copolymer/homopolymer blend with 80.0 vol% lamellar-forming PS-*b*-PMMA and 20.0 vol% cross-linkable homopolymers x-PS and x-PMMA (note that these are not truly homopolymers but rather random copolymers with 1 mol% concentrations of a reactive epoxy functionality, but, for clarity, they are labeled as such throughout). The relative amount of x-PS and x-PMMA added was carefully tuned to control the final volume fractions of PS and PMMA in the block copolymer blends. Three different block copolymer compositions ($\phi_{PS}$ = 40, 50, or 60 vol%) were considered for the layers, but each self-assembled into lamellar structures with similar periodicities ($L_0$ = 56–58 nm) (see Supporting Information Figure S1). It is important to comment, however, that for the materials presented here, the block copolymer and homopolymers are not cross-linked together and, given sufficient time, the block copolymer could be mixed within the layers or completely extracted. Future implementation of these systems may benefit from cross-linkable block copolymers that can be directly reacted into the molecular network to fully inhibit mixing between layers and make the structures insoluble (although in some cases this might be undesirable, for example in the PS nanostructures used for lift-off as detailed below).

**Figure 3** shows top-down scanning electron microscopy (SEM) images of 50–40PS and 50–60PS bilayer films after removal of the PMMA domain, as well as a single layer 50PS film of equivalent total thickness. The light regions in the SEM images correspond to the PS nanostructures. The formation of lamellar structures was observed throughout indicating that the block copolymer self-assembled in the top layer matched and was registered with the pattern in the underlying layer, which for these systems had an identical composition. The top-down SEM images from the 50–40PS to 50–60PS bilayers also exhibit the visual trend that the PS domains become wider while the PMMA domains become narrower, which is consistent with the profiles targeted in these bilayer thin films. On the right side of Figure 3, an analysis of the grayscale top-down SEM images confirms this trend. Histograms of the grayscale color of each

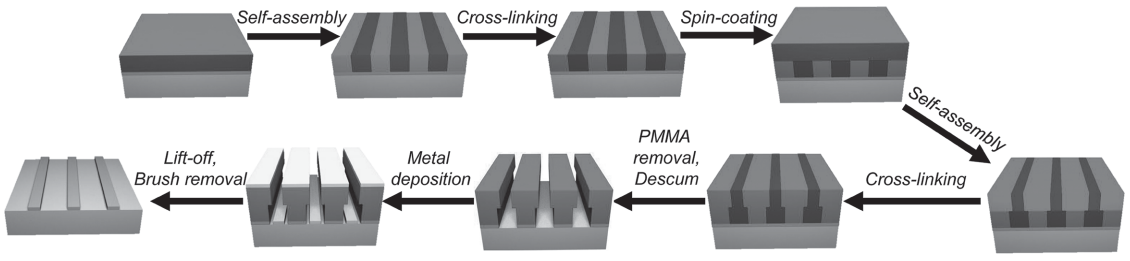


**Figure 2.** Step-by-step process flow to achieve a bilayer undercut profile in self-assembled block copolymer nanostructures.

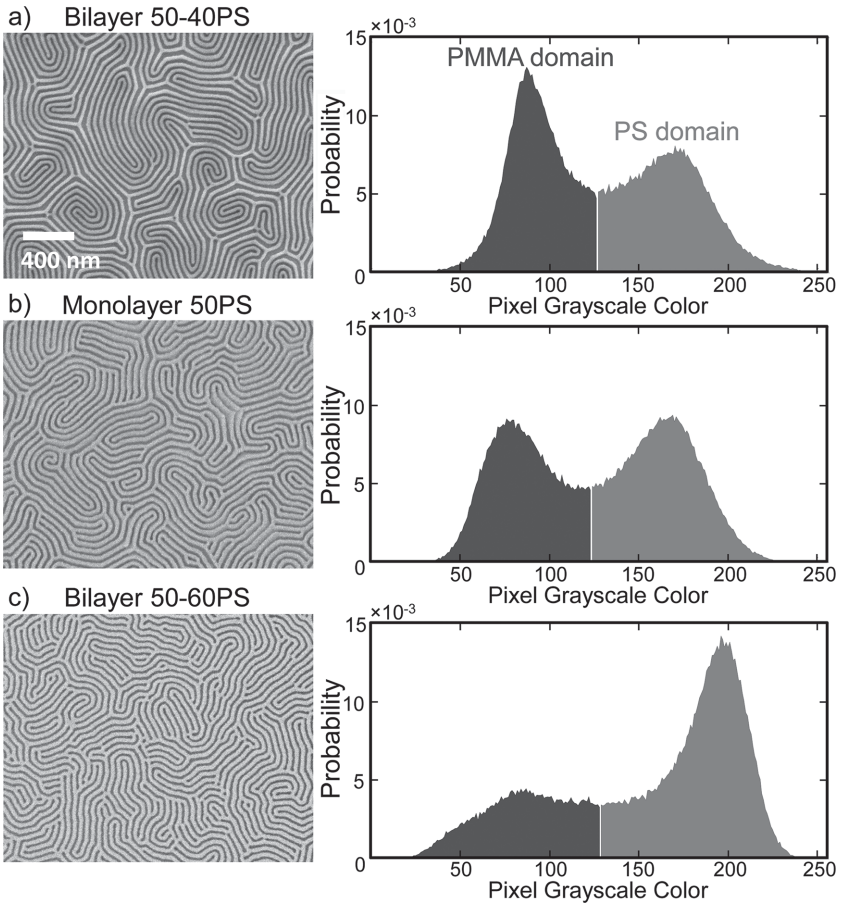


**Figure 3.** Top-down SEM images (left) and the corresponding histograms of grayscale color (right) for bilayer block copolymer films with top layer polystyrene compositions of a) 40, b) 50, and c) 60 vol%. The dark gray and light gray shaded areas indicate the pixels assigned to belong to the PMMA and PS domains in the SEM image, respectively. Note that in this case the PMMA domains were removed prior to SEM imaging.

pixel in the images were determined and have two clear peaks corresponding to the PMMA (dark, low grayscale color) and PS (light, high grayscale color) domains. In order to quantify the relative composition of each domain at the top surface of the bilayer film, a threshold was applied corresponding to the minimum probability between the two peaks in the distribution. **Table 1** summarizes the measured PS and PMMA compositions at the top surface of the films, which ranged from 44 to 70 vol% PS and closely matched the targeted surface compositions of 40 to 60 vol% PS (for 50–40PS to 50–60PS, respectively).

**Table 1.** The areal fraction of PS and PMMA at the free surface of the block copolymer bilayer films as determined by top-down SEM imaging.

| 3D structure design (as denoted by PS composition)[a)] | Measured PS composition at the film surface [vol%] | Measured PMMA composition at the film surface [vol%] |
|---|---|---|
| Bilayer 50–40PS | 46% ± 2% | 54% ± 2% |
| Monolayer 50PS | 54% ± 1% | 46% ± 1% |
| Bilayer 50–60PS | 70% ± 1% | 30% ± 1% |

[a)]Notation "50–40PS" means the multilayer structure was built with a bottom layer consisting of 50 vol% PS and 50 vol% PMMA and a top layer of 40 vol% PS and 60 vol% PMMA.

One domain of the block copolymer nanostructures must be selectively removed to fabricate masks or templates suitable for pattern transfer processes such as lift-off. Here the PMMA domain of the lamellar nanostructures in the bilayer film was selectively removed by exposure to UV light (254 nm, 1 J $cm^{-2}$) and development in acetic acid (a non-solvent for the PS domain).[18b] The remaining PS template was then descummed by a short oxygen plasma treatment. Subsequently an adhesion layer of 1.0 nm of Cr and 5.0 nm of Au was deposited by thermal evaporation.

The undercut profile achieved by the bilayer 50–60PS film is evidenced in the cross-sectional SEM images of **Figure 4**. Figure 4a shows the cross-sectional SEM image of bilayer 50–60PS after descumming by oxygen plasma treatment, while Figure 4b shows the same structures after metal deposition. The designed undercut structure is evident in both images, although cross-sectional imaging of the polymer nanostructures alone is difficult and subject to charging and changes in shape due to surface melting. The metal coated structures in Figure 4b provide a better indication of the T-topped shaped structures achieved by this 50–60PS bilayer system and the flat topped surfaces of the nanostructures. The sidewall angle of the undercut profile was measured to be 7° ± 3° from the substrate normal for the 50–60PS bilayer system (by linear fitting of the line edges in Figure 4b), which is close to that predicted through strictly volumetric arguments for this bilayer composition (≈11°) and substantially different from the perpendicular interfaces achieved in the monolayer block copolymer system. Notably such features of the bilayer nanostructures are able to withstand the descumming process, which uses an isotropic $O_2$ plasma that likely etches such corners and surfaces more rapidly.[19] Most importantly for lift-off processes, the undercut profile leads to breaks in the continuity of the deposited metal film, such that minimal metal on the photoresist sidewalls and gaps at the bottom of the photoresist layer are clearly observed (in Figure 4b as indicated with white arrows). These discontinuities in the deposited metal layer allows solvent (in this case toluene) to penetrate and dissolve the sacrificial PS template, as well as to enable the unconnected metal to freely lift-off the surface.

Characterization of the metal lift-off process using the bilayer block copolymer nanostructures with controlled sidewall profiles was performed as shown in **Figure 5** and **6**. Metal films were deposited on the PS templates on Si wafer or glass slide substrates, and lift-off was performed by sonicating the samples in a toluene bath at 55 °C. Improvements in the lift-off process achieved using the undercut profile self-assembled by the

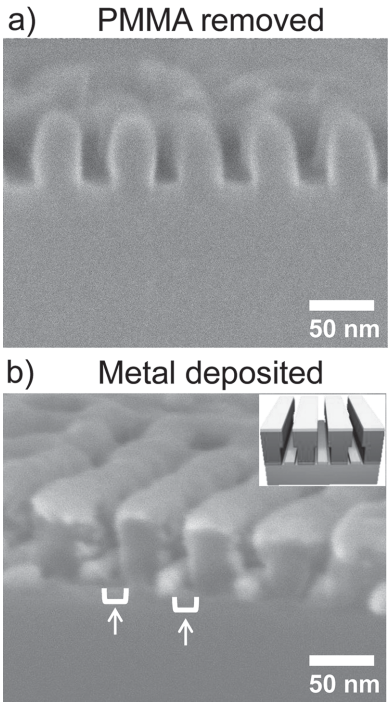


**Figure 4.** Cross-sectional SEM images of bilayer 50–60PS films with undercut profiles: a) the PS mask remaining after the PMMA domain is removed and b) the Cr and Au metal film deposited on the PS mask, with two breaks or gaps in the film continuity highlighted with the white arrows.

50–60PS bilayer system were compared to systems with vertical (50PS monolayer) and positive (50–40PS bilayer) sidewall profiles. Figure 5a shows defect-free metal nanowires (25 nm wide, 6 nm thick) fabricated by lift-off for 600 min using the undercut 50–60PS bilayer structures. In contrast, under identical lift-off conditions, the PS templates with vertical (Figure 5b) or positive (not shown) sidewall profiles exhibited retention and did not allow for complete lift-off, as indicated by substantial portions of the substrate remaining blanketed with metal coating the PS template.

The progress of the lift-off process over large areas can be characterized optically as shown in Figure 6 for the three bilayer block copolymer structures with distinct sidewall profiles. The extent of lift-off was studied by monitoring the UV–vis transmittance (as reported at a wavelength of 495 nm) as a function of the lift-off time (measured every 15 min). As indicated in the transmittance spectra across the UV–vis range, the wavelength of 495 nm corresponds to the maximum transmittance, whereas ≈580 nm corresponds to a minimum in transmittance that results from the localized surface plasmon resonance (LSPR) for such Au nanostructures. While either wavelength could be used to monitor the extent of metal liftoff as a function of time, transmittance at 495 nm has been reported to decouple the extent of liftoff from the LSPR response that depends on structure size and spacing which varies throughout the liftoff process.

The optical data in Figure 6 has a number of interesting features. First, lift-off was completed in ≈450 min when using the PS masks with an undercut profile (Bilayer 50–60PS), which is

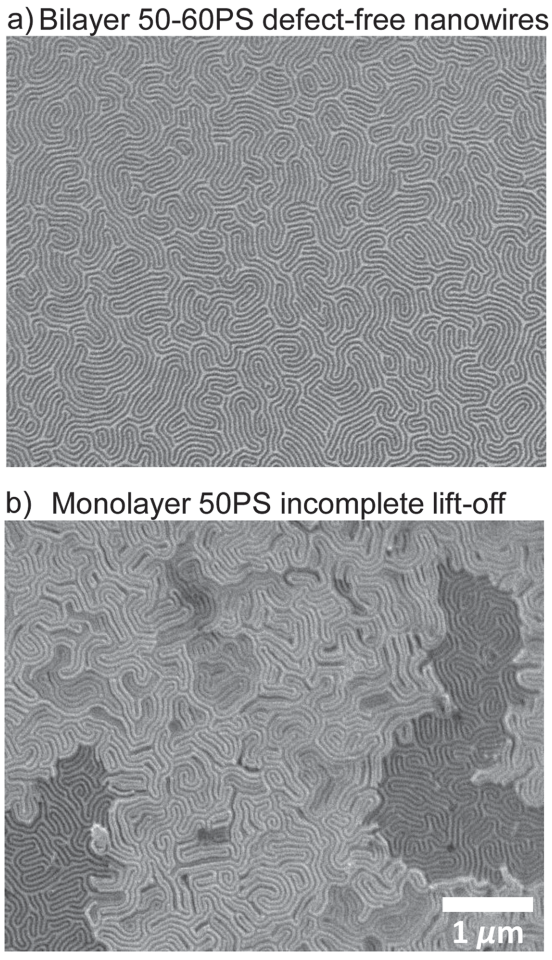


**Figure 5.** Top-down SEM images of metal nanowires after a) successful and b) incomplete lift-off. Under identical lift-off conditions (sonication at 55 °C for 10 h) a) a block copolymer template with an undercut profile (bilayer 50–60PS film) achieves complete lift-off and defect-free pattern transfer, whereas b) a block copolymer template without an undercut profile (monolayer 50PS film) does not allow for successful lift-off (the dark regions on the bottom left and right show the desired outcome, while the remaining brighter areas have not been successfully lifted-off and have metal blanketing the PS template).

approximately an order of magnitude faster than the masks with a positive sidewall profile (≈4000 min). Furthermore no significant lift-off was observed until ≈600 min for the templates with a vertical or positive sidewall profile. The significantly faster rates of lift-off achieved with sidewall control are important for potential pattern transfer processes and nanomanufacturing using block copolymers in thin films. Second, there is a period for all samples before which there is no change in transmittance as a function of lift-off time. This induction period likely corresponds, in part, to the time necessary for the solvent to access the PS template and solubilize it. Finally, the transmittance remains constant after lift-off is complete and has very low variation across the sample surface. From this observation, it can be concluded that the metal nanowires are homogeneous across the substrate (in terms of the extent of lift-off and the film thickness) and that adhesion of the metal nanowires to the substrate is strong.

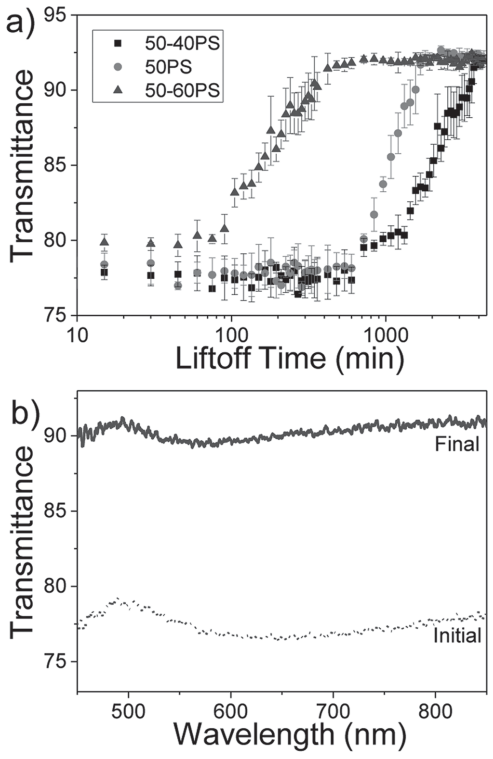


**Figure 6.** a) Transmittance at 495 nm of the Au coated block copolymer nanostructures during the course of the lift-off process as a function of sonication time. The error bars represent 1$\sigma$ variation of three measurements taken across the sample. b) Transmittance spectra for the 50–60PS system before and after completion of the metal lift-off process.

## 3. Conclusions

In summary, we have presented a simple approach to control the sidewall profile of block copolymer nanostructures self-assembled in thin films and demonstrated the ability of such profile control to enhance lift-off pattern transfer processes. The approach utilizes bilayer block copolymer films, with each layer having a well-defined composition and characteristic dimension, and is analogous to profile control techniques developed for commercial photoresists and lithographic processes. The improved liftoff process detailed in this manuscript will simplify the transfer of such block copolymer patterns into functional metallic or semiconducting materials, or even into other sacrificial layers. For example, we have used this lift-off process to deposit thin Cr or alumina hard masks for anisotropic reactive ion etching and achieved high aspect ratio (>5) features etched into Si substrates. The proof-of-concept demonstration presented here can easily be scaled to smaller dimensions, implemented in cylinder-forming systems, or adapted to other block copolymer materials. The processes and materials used here are also compatible with conventional nanofabrication tools,[20] including those being developed specifically for block copolymer lithography (e.g., tools for solvent vapor annealing) and directed self-assembly such as with chemically patterned substrates.[16b–e] Experiments and mean-field simulations on the directed self-assembly of PS-*b*-PMMA lamellae on chemically patterned surfaces indicate that the domain interface depends strongly on the film thickness and the mismatch in periodicity between the block copolymer and the surface pattern.[12a] Thus, optimization of the sidewall profile of block copolymer nanostructures may be expanded to other applications, in the future, by controlling the thickness of each layer or the use of multilayer (3 or more layers) films to create complex, 3D profiles.

## 4. Experimental Section

*Processing of Bilayer Block Copolymer Thin Films*: A neutral substrate for the self-assembly of lamellar-forming PS-b-PMMA block copolymers with perpendicular orientations was prepared by coating a P(S-r-MMA-r-GMA) random copolymer brush onto Si substrates. Si wafers were purchased from Montco Silicon and piranha treated with a mixture of 30% $H_2O_2$/70% $H_2SO_4$ (v/v) at 70 °C for 20 min. The cleaned substrates were rinsed extensively with distilled water, and then further rinsed with acetone and toluene. The random copolymer was synthesized by free-radical polymerization from styrene, methyl methacrylate, and glycidyl methacrylate monomers to achieve a final molar composition of 58% styrene, 31% methyl methacrylate, and 1% glycidyl methacrylate as confirmed by $^1$H-NMR. A 0.3 wt% solution of the random copolymer in anhydrous toluene (EMD Chemicals, 99.8 wt%) was prepared and spincast to a film thickness of 10 nm onto the clean silicon wafers. Annealing at 170 °C for 4 h cross-linked the random copolymer into a dense mat, and subsequent sonication in a toluene bath removed unreacted polymer. Thin films of PS-*b*-PMMA block copolymer and block copolymer/homopolymer blends were spincast onto the prepared neutral surfaces. The lamellar-forming block copolymer (PS-*b*-PMMA, 47k:53k, PDI = 1.12) was purchased from Polymer Source, Inc. Homopolymers with a low concentration of thermally cross-linkable functionality were synthesized through atom transfer radical polymerization.[21] These cross-linkable homopolymers included x-PS (17.4 kDa, PDI = 1.28) and x-PMMA (25.2 kDa, PDI = 1.47) each with 1 mol% of glycidyl methacrylate functionality randomly incorporated. Solutions of block copolymer and homopolymer were prepared at a concentration of 1.5 wt% by weighing out dry polymer and adding toluene dropwise. Three blend solutions of block copolymer and cross-linkable homopolymer were prepared by blending the solutions of block copolymer and homopolymer as indicated in **Table 2**, targeting different total volume fractions of styrene and methyl methacrylate in each solution, but identical volume fractions of homopolymer. The ≈50 nm monolayer block copolymer thin film was produced by spincasting (5000 rpm for 30 s) a 1.5 wt% solution. Each ≈25 nm thick layer in the bilayer block copolymer thin films was achieved using block copolymer blend solutions diluted to 0.75 wt% concentrations and spincasting (4000 rpm for 45 s). Solvent vapor annealing was performed by exposing the block copolymer thin films to a saturated vapor of mixed solvents. Acetone (30 mL, Fisher, 99%) and cyclohexane (30 mL, Fisher, 99%) were added to the bottom of a glass desiccator (1.5 L volume). The solvents were degassed under house vacuum (25 Torr) to remove any dissolved gases prior to solvent annealing. The thin film samples were suspended on a metal frame above the solvent mixture. The system pressure was then lowered to 20 Torr, the desiccator was sealed, and the polymer thin films were swollen in the mixed solvent environment for 2 h. The solvent vapor

**Table 2.** Block copolymer blends with controlled volume fractions of PS.

| | 40PS | 50PS | 60PS |
|---|---|---|---|
| 1.5 wt% PS-b-PMMA [mL] | 2.000 | 2.000 | 2.000 |
| 1.5 wt% x-PS [mL] | 0 | 0.237 | 0.471 |
| 1.5 wt% x-PMMA [mL] | 0.529 | 0.263 | 0 |
| Total volume fraction of PS | 40.0% | 50.0% | 60.0% |
| Volume fraction of homopolymer | 20.0% | 20.0% | 20.0% |

annealing process was quenched by opening the chamber to vacuum to remove solvent vapor and followed by opening the entire chamber to air to allow the swollen block copolymer thin films to dry. Subsequently, the solvent vapor annealed samples were thermally treated (190 °C for 1 h under ≈10 Torr vacuum) to remove residual solvent, improve microphase separation of the self-assembled structures, and to complete the thermally activated cross-linking reaction. This process for deposition and self-assembly was then repeated for a second layer (≈25 nm film) of block copolymer, in some cases using block copolymer systems of identical composition and in other cases with block copolymer systems of differing composition.

*Pattern Transfer to Metal Nanostructures via a Lift-Off Process*: The block copolymer thin film samples were exposed to UV light (UVP CL-1000 ultraviolet cross-linker at $\lambda = 254$ nm and an exposure dose of 1 J cm$^{-2}$) and rinsed in acetic acid to remove the PMMA domain.[18b] The remaining PS template was descummed by an oxygen plasma treatment (gas: $O_2$, flow rate: 5 SCCM, pressure: 150 mTorr, power: 40 W) to remove residual PMMA and the brush layer used for surface treatment. Metal thin films consisting of 1 nm Cr and 5 nm Au were evaporated sequentially using a CVC 3-boat thermal evaporator. The lift-off process was carried out by sonicating (Fisher Scientific FS30H ultrasonic cleaner) the metal deposited samples in toluene at 55 °C. The samples were dried in a stream of $N_2$ prior to SEM imaging.

*Nanostructure Characterization*: The block copolymer morphology in thin films and the metal nanostructures were imaged by scanning electron microscopy (SEM) using a JEOL JSM-7401F. Top-down SEM images were collected using gentle beam mode operating at an accelerating voltage of 1 kV and a gun emission current of ≈10 mA. Samples for cross-sectional SEM imaging were cleaved in liquid nitrogen. Cross-sectional SEM images were collected with the sample tilted at 80° from the sample normal using an accelerating voltage of 5 kV.

*Optical Characterization of Extent of Lift-Off*: The extent of lift-off was determined by transmission measurements (light source: Mikropack HL-2000-FHSA, detector: Ocean Optics USB4000) using metal films deposited on glass slides. Note that the block copolymer processing was identical on the glass substrates (pre-cleaned Fisher Scientific plain microscope slides) as it was on the Si substrates. A glass slide with a 10 nm layer of neutral brush was used as bright reference spectrum for the transmission measurements, i.e., corresponding to 100% transmission. Transmission measurements (beam spot with a diameter of ≈3.0 mm) were collected at three distinct locations across the substrate, thus allowing for the extent of lift-off to be quantified across large areas.

## Supporting Information

Supporting Information is available from the Wiley Online Library or from the author.

## Acknowledgements

This research was supported by the University of Colorado and the Colorado Nanofabrication Laboratory through the National Science Foundation (Grant No. ECS-0335765). This work was performed in part at the University of Colorado's Nanomaterials Characterization Facility.

Received: June 3, 2014
Revised: August 4, 2014
Published online: September 10, 2014

[1] a) R. R. Li, P. D. Dapkus, M. E. Thompson, W. G. Jeong, C. Harrison, P. M. Chaikin, R. A. Register, D. H. Adamson, *Appl. Phys. Lett.* **2000**, *76*, 1689; b) C. T. Black, K. W. Guarini, K. R. Milkove, S. M. Baker, T. P. Russell, M. T. Tuominen, *Appl. Phys. Lett.* **2001**, *79*, 409; c) P. S. Jo, J. Sung, C. Park, E. Kim, D. Y. Ryu, S. Pyo, H. C. Kim, J. M. Hong, *Adv. Funct. Mater.* **2008**, *18*, 1202; d) H. C. Kim, S. M. Park, W. D. Hinsberg, *Chem. Rev.* **2010**, *110*, 146.

[2] a) C. Osuji, C. Y. Chao, I. Bita, C. K. Ober, E. L. Thomas, *Adv. Funct. Mater.* **2002**, *12*, 753; b) Z. H. Nie, E. Kumacheva, *Nat. Mater.* **2008**, *7*, 277.

[3] a) C. De Rosa, C. Park, E. L. Thomas, B. Lotz, *Nature* **2000**, *405*, 433; b) J. Y. Cheng, C. A. Ross, V. Z. H. Chan, E. L. Thomas, R. G. H. Lammertink, G. J. Vancso, *Adv. Mater.* **2001**, *13*, 1174; c) J. Y. Cheng, C. A. Ross, E. L. Thomas, H. I. Smith, R. G. H. Lammertink, G. J. Vancso, *IEEE T. Magn.* **2002**, *38*, 2541; d) V. P. Chuang, J. Gwyther, R. A. Mickiewicz, I. Manners, C. A. Ross, *Nano Lett.* **2009**, *9*, 4364; e) G. L. Liu, P. F. Nealey, R. Ruiz, E. Dobisz, K. C. Patel, T. R. Albrecht, *J. Vac. Sci. Technol. B* **2011**, 29; f) R. Ruiz, E. Dobisz, T. R. Albrecht, *ACS Nano* **2011**, *5*, 79.

[4] C. C. Liu, P. F. Nealey, Y. H. Ting, A. E. Wendt, *J. Vac. Sci. Technol. B* **2007**, *25*, 1963.

[5] a) C. M. Bates, M. A. B. Pantoja, J. R. Strahan, L. M. Dean, B. K. Mueller, C. J. Ellison, P. F. Nealey, C. G. Willson, *J. Polym. Sci. Pol. Chem.* **2013**, *51*, 290; b) Y. H. Ting, S. M. Park, C. C. Liu, X. S. Liu, F. J. Himpsel, P. F. Nealey, A. E. Wendt, *J. Vac. Sci. Technol. B* **2008**, *26*, 1684.

[6] M. J. Madou, *Fundamentals of Microfabrication*, CRC Press, Boca Raton, FL **2009**.

[7] A. Mayer, N. Bogdanski, S. Mollenbeck, K. Dhima, M. Papenheim, H. C. Scheer, *J. Vac. Sci. Technol. B* **2010**, *28*, C6m136.

[8] G. Y. Jung, W. Wu, S. Ganapathiappan, D. A. A. Ohlberg, M. S. Islam, X. Li, D. L. Olynick, H. Lee, Y. Chen, S. Y. Wang, W. M. Tong, R. S. Williams, *Appl. Phys. A* **2005**, *81*, 1331.

[9] a) J. W. Chang, C. P. Chen, *Adv. Resist Technol. Processing XXI, Parts 1 and 2* **2004**, *5376*, 967; b) H. S. Lee, J. B. Yoon, *J. Micromech. Microeng.* **2005**, *15*, 2136; c) A. Voigt, M. Heinrich, K. Hauck, R. Mientus, G. Gruetzner, M. Topper, O. Ehrmann, *Microelectron. Eng.* **2005**, *78*, 503; d) J. Minter, M. Ross, W. R. Livesay, S. Wong, M. Narcy, T. Marlowe, *Microlithography 1999: Adv. Resist Technol. Processing XVI, Parts 1 and 2* **1999**, *3678*, 1074.

[10] a) C. P. Chen, J. W. Chang, R. Kaji, H. Kawasaki, *Emerging Lithographic Technol. IX, Pts 1 and 2* **2005**, *5751*, 601; b) H. Y. Jung, S. Y. Hwang, B. J. Bae, H. Lee, *J. Vac. Sci. Technol. B* **2009**, *27*, 1861; c) H. F. Yang, A. Z. Jin, Q. Luo, J. J. Li, C. Z. Gu, Z. Cui, *Microelectron. Eng.* **2008**, *85*, 814.

[11] a) G. H. Fredrickson, *Macromolecules* **1994**, *27*, 7382; b) Y. Rharbi, M. A. Winnik, *Macromolecules* **2001**, *34*, 5238.

[12] a) E. W. Edwards, M. Muller, M. P. Stoykovich, H. H. Solak, J. J. de Pablo, P. F. Nealey, *Macromolecules* **2007**, *40*, 90; b) G. M. Perera, C. Q. Wang, M. Doxastakis, R. J. Kline, W. L. Wu, A. W. Bosse, G. E. Stein, *ACS Macro Lett.* **2012**, *1*, 1244.

[13] a) J. Y. Cheng, A. M. Mayes, C. A. Ross, *Nat. Mater.* **2004**, *3*, 823; b) M. P. Stoykovich, H. Kang, K. C. Daoulas, G. Liu, C. C. Liu, J. J. de Pablo, M. Mueller, P. F. Nealey, *ACS Nano* **2007**, *1*, 168.

[14] a) K. C. Daoulas, M. Muller, M. P. Stoykovich, H. Kang, J. J. de Pablo, P. F. Nealey, *Langmuir* **2008**, *24*, 1284; b) G. E. Stein, J. A. Liddle, A. L. Aquila, E. M. Gullikson, *Macromolecules* **2010**, *43*, 433; c) M. P. Stoykovich, K. C. Daoulas, M. Muller, H. M. Kang, J. J. de Pablo, P. F. Nealey, *Macromolecules* **2010**, *43*, 2334; d) P. N. Patrone, G. M. Gallatin, *Macromolecules* **2012**, *45*, 9507; e) A. J. Peters, R. A. Lawson, P. J. Ludovice, C. L. Henderson, *J. Vac. Sci. Technol. B* **2013**, *31*, 06F302.

[15] I. P. Campbell, C. L. He, M. P. Stoykovich, *ACS Macro Lett.* **2013**, *2*, 918.

[16] a) H. Jung, D. Hwang, E. Kim, B. J. Kim, W. B. Lee, J. E. Poelma, J. Kim, C. J. Hawker, J. Huh, D. Y. Ryu, J. Bang, *ACS Nano* **2011**,

*5*, 6164; b) S. O. Kim, H. H. Solak, M. P. Stoykovich, N. J. Ferrier, J. J. de Pablo, P. F. Nealey, *Nature* **2003**, *424*, 411; c) M. P. Stoykovich, M. Muller, S. O. Kim, H. H. Solak, E. W. Edwards, J. J. de Pablo, P. F. Nealey, *Science* **2005**, *308*, 1442; d) L. Rockford, Y. Liu, P. Mansky, T. P. Russell, M. Yoon, S. G. J. Mochrie, *Phys. Rev. Lett.* **1999**, *82*, 2602; e) Y. Tada, S. Akasaka, H. Yoshida, H. Hasegawa, E. Dobisz, D. Kercher, M. Takenaka, *Macromolecules* **2008**, *41*, 9267; f) X. M. Yang, L. Wan, S. G. Xiao, Y. A. Xu, D. K. Weller, *ACS Nano* **2009**, *3*, 1844.

[17] J. N. L. Albert, T. H. Epps, *Mater. Today* **2010**, *13*, 24.

[18] a) T. Thurn-Albrecht, R. Steiner, J. DeRouchey, C. M. Stafford, E. Huang, M. Bal, M. Tuominen, C. J. Hawker, T. P. Russell, *Adv. Mater.* **2000**, *12*, 787; b) S. J. Jeong, G. D. Xia, B. H. Kim, D. O. Shin, S. H. Kwon, S. W. Kang, S. O. Kim, *Adv. Mater.* **2008**, *20*, 1898.

[19] F. Hamaoka, T. Yagisawa, T. Makabe, *J. Phys. D Appl. Phys.* **2009**, *42*.

[20] a) C. J. Hawker, T. P. Russell, *MRS Bull.* **2005**, *30*, 952; b) M. P. Stoykovich, P. F. Nealey, *Mater. Today* **2006**, *9*, 20; c) E. L. Schwartz, J. K. Bosworth, M. Y. Paik, C. K. Ober, *Adv. Resist Mater. Processing Technol. XXVII, Parts 1 and 2* **2010**, *7639*; d) S. J. Jeong, J. Y. Kim, B. H. Kim, H. S. Moon, S. O. Kim, *Mater. Today* **2013**, *16*, 468; e) C. M. Bates, M. J. Maher, D. W. Janes, C. J. Ellison, C. G. Willson, *Macromolecules* **2014**, *47*, 2.

[21] a) M. Kamigaito, T. Ando, M. Sawamoto, *Chem. Rev.* **2001**, *101*, 3689; b) K. Matyjaszewski, J. H. Xia, *Chem. Rev.* **2001**, *101*, 2921.